Atomic Data Needs for X-ray Astronomy. 22 June 2000
http://heasarc.gsfc.nasa.gov/docs/heasarc/atomic/
M. A. Bautista, T. R. Kallman, and A. K. Pradhan, eds.

Distorted Wave Calculations and Applications

A. K. Bhatia
Laboratory for Astronomy and Solar Physics
NASA/Goddard Space Flight Center
Greenbelt, Maryland 20771
USA

Abstract. Physical properties such as temperature and electron density of solar plasma and other astrophysical objects can be inferred from EUV and X-ray emission lines observed from space. These lines are emitted when the higher states of an ion are excited by electron impact and then decay by photon emission. Excitation cross sections are required for the spectroscopic analyses of the observations and various approximations have been used to calculate the scattering functions. One of them which has been widely used is a distorted wave approximation. This approximation, along with its applications to solar observations, is discussed. The Bowen fluorescence mechanism and optical depth effects are also discussed. It is concluded that such calculations are reliable for highly charged ions and for high electron temperatures.

1. Introduction

Since this workshop is dedicated to X-ray astronomy it is appropriate to mention that solar X-rays were first detected on August 5, 1948 from a V2 rocket and the first nonsolar X-ray source was also discovered from a rocket flight in 1962. Since then a number of satellites have been launched to study X-ray sources, the most recent satellites being the *Chandra* and the $XMM-Newton$ observatories. Photons from the Sun and other astrophysical objects are messengers bearing information about the plasma properties of these objects. The purpose of the distorted wave (DW) calculations is to provide atomic data required to infer the plasma properties such as electron density, temperature, and elemental abundances (which in the solar corona and solar winds are different from their photospheric values). This difference in elemental abundances seems to be a function of the first ionization potential (FIP) of the elements and can vary from region to region of the Sun. Other properties of interest are heating of stellar coronae, magnetic fields, and acceleration of stellar winds.

Photons are emitted when the upper levels of an ion excited by electron impact decay to the lower levels. Some of the high-lying levels can be populated by charge exchange and some levels can be populated by the dielectronic recombination of electrons with ions. Excitation by heavy particles like protons can be important for the fine-structure levels but most of the time electron impact excitations dominate. This is called "the coronal condition", i.e. electron impact excitation is balanced by radiative decay. For an optically thin plasma, the intensity of the observed line due to the transition from level j to level i is given by

$$I_{ji} = N_j A_{ji} \Delta E_{ij} \tag{1}$$

where N_j is the population of the upper level and depends on the electron density N_e, A_{ji} is the spontaneous radiative transition rate, and ΔE_{ij} is the energy separation between the two levels. In general, the ionization and recombination processes are very slow compared to excitation processes. This implies that excitation processes can be considered separately from ionization and recombination processes. Therefore, assuming ionization equilibrium, the level population of a multi-level ion excited by electron impact is obtained by solving the statistical equilibrium equations

$$\frac{dN_i}{dt} = -N_e N_i \sum_{j>i} C^e_{ij} + \sum_{j>i} N_j A_{ji} - N_i \sum_{j<i} A_{ij} + N_e \sum_{j>i} N_j C^d_{ji} \tag{2}$$

$$\frac{dN_i}{dt} = 0 \quad \text{for steady state} \tag{3}$$

where C^e_{ij}, for an assumed Maxwellian electron velocity distribution at temperature T_e for an isothermal plasma, is the excitation rate coefficient from level i to level j and is given by

$$C^e_{ij} = \frac{8.63 \times 10^{-6}}{\omega_i k T_e^{1.5}} \int_{\Delta E_{ij}}^{\infty} \Omega_{ij}(E) \exp(-\frac{E}{kT_e}) dE \tag{4}$$

where k is the Boltzmann constant and the units are cm^3 sec^{-1}. The thermally averaged collision strength is called the effective collision strength Υ_{ij} defined as

$$\Upsilon_{ij} = \int_0^{\infty} \Omega_{ij}(E) \exp(-\frac{E}{kT_e}) d(\frac{E}{kT_e}) \tag{5}$$

so that

$$C^e_{ij} = \frac{8.63 \times 10^{-6}}{\omega_i T_e^{0.5}} \Upsilon_{ij}(T_e) \exp(-\frac{\Delta E_{ij}}{kT_e}) \tag{6}$$

The deexcitation rate coefficient C^d_{ji} is obtained by the principle of detailed balance:

$$C^d_{ji} = \frac{\omega_i}{\omega_j} \exp(\frac{\Delta E_{ij}}{kT_e}) C^e_{ij} \tag{7}$$

The dimensionless quantity $\Omega_{ij} = \Omega_{ji}$ is the collision strength which we want to calculate. This is related to the excitation cross section σ_{ij} for exciting the target state i to the state j

$$\sigma_{ij} = \frac{\pi a_0^2}{\omega_i k_i^2} \Omega_{ij} \tag{8}$$

at wave number k_i of the incident electron; ω_i is the statistical weight of the initial target state and Ry units are used throughout. At low electron density most of the population is in the ground level i=1 and if only one level is excited then j=2, and Equations (2) and (3) reduce to

$$N_e N_1 C^e_{12} = N_2 A_{21} \tag{9}$$

where C^d_{12} has been neglected because it is very small compared to A_{21}. The radiative transition rates due to dipole-allowed transitions are much higher than electric quadrupole, magnetic dipole, and quadrupole transition rates. The observed transitions are classified as resonance or dipole-allowed transitions (spin-allowed and angular momentum changes by 1), forbidden transitions (spin-forbidden and no change in angular momentum), and intercombination transitions (spin-forbidden and the angular momentum changes). For a known Z dependence, the radiative rates can be scaled along the isoelectronic series. The rates for the electric-dipole, electric-quadrupole, and magnetic-dipole are proportional to Z^4, Z^6, and Z^{10}, respectively. The magnetic-dipole rates can become comparable to the electric-dipole rates at high Z. This then gives lines due to magnetic-dipole transitions as intense as the lines due to electric-dipole transitions for high Z ions.

If the density is very low then the collisional excitation becomes less important and recombination of electrons and ions in high-lying levels becomes more important. Emission lines are then due to cascades to lower levels.

If the electron density is very high ($N_e > 10^{18} cm^{-3}$) as in stellar envelopes, then Equations (2) and (3) in the two-level model give

$$N_1 C^e_{12} = N_2 C^d_{21} \tag{10}$$

which is the condition for thermodynamic equilibrium. Using Equation (7), Equation (10) reduces to

$$\frac{N_2}{N_1} = \frac{\omega_2}{\omega_1} \exp(-\frac{\Delta E_{12}}{kT_e}) \tag{11}$$

This is the Saha-Boltzmann distribution indicating that at very high electron densities the level populations are proportional to their weights. This can be generalized to all the levels of the ion. At such high densities the optical properties of the plasma can be considered separately because the statistical equilibrium equations need not be solved for the level populations. This condition is called local thermodynamic equilibrium (LTE).

2. Calculations

The simplest approximation is to use Coulomb waves for the incident and scattered electron in the expression for the transition matrix element

$$f_{ij} \propto < \Psi_j \, |V| \, \Psi_i > \tag{12}$$

where f_{ij} is the transition amplitude, Ψ_i and Ψ_j are the initial and final state wavefunctions, and V is the perturbing potential. In general, the electrons in the ions are moving faster than the incident electron and Born-type approximations are not valid. The next step is to solve the scattering problem accurately. The total wave function is of the form

$$\Psi_i = A\Phi_i(1, 2, ..., N)F_i(N+1) \tag{13}$$

where Φ_i is the target function, F_i represents the incident or the scattered electron, and A is the antisymmetrization operator. The Hamiltonian of the (N+1)-electron system is given by

$$H_{N+1} = -\sum_i (\nabla_i^2 + \frac{2Z}{r_i}) + \sum_{i>j} \frac{2}{r_{ij}} \tag{14}$$

The wave function Ψ_i satisfies the Schrödinger equation

$$H_{N+1}\Psi_i = E\Psi_i \tag{15}$$

In the DW approximation the coupling between the channels (target+scattered electron) is neglected. For this reason resonances, representing compound states of the target and the electron, cannot be included in such calculations, and a close-coupling approximation is required to include resonances, but then the scattering equations are coupled integro-differential equations. The solution of integral equations requires a lot more computer time than is required by DW equations. Since the resonance contribution cannot be scaled along the isoelectronic series, it is not possible to scale effective collision strengths obtained in the close-coupling or R-matrix approximations while those obtained in the DW approximation can be scaled. The resonance contribution to the effective collision strength is often more important for the forbidden and intercombination transitions than for the dipole-allowed transitions. For the latter transitions the contribution from the incident partial waves can be much more substantial than the contribution from resonances.

In the DW approximation, the scattering function satisfies the equation

$$\left[\frac{d^2}{dr^2} - \frac{l_i(l_i+1)}{r^2} + \frac{2z}{r} + V_i(r) + k_i^2\right] F_i(r) = 0 \tag{16}$$

where z=Z-N is the ion charge, Z being the nuclear charge and N the number of electrons, and $V_i(r)$ is a central potential. The $F_i(r)$ satisfies the boundary conditions

$$F_i(0) = 0 \tag{17}$$

$$F_i(r \to \infty) = \frac{1}{k_i^{0.5}} \sin[k_i r - \frac{l_i \pi}{2} + \frac{z}{k_i} ln(2k_i r) + arg\Gamma(l_i + 1 - \frac{iz}{k_i}) + \delta_{l_i}] \tag{18}$$

where δ_{l_i} is the phase shift in addition to the Coulomb phase shift.

Along these lines DW programs (Eissner and Seaton 1979; Eissner 1998) have been developed at University College London (UCL), and in these programs $V_i(r)$ is chosen as a scaled Thomas-Fermi-Dirac-Amaldi potential. There are a number of excited states of the target and equations like Equation (16) have to be solved for each state. The reaction matrix is given by

$$K_{ij} = - < \Psi_j \, |H_{N+1} - E| \, \Psi_i > \tag{19}$$

and the T-matrix is given by

$$T = -\frac{2iK}{1+iK} \tag{20}$$

The collision strength for total angular momentum L, spin S, and parity π is given by

$$\Omega_{ij}^{LS\pi} = \frac{(2L+1)(2S+1)}{2} \sum_{l_i l_j} |T|^2 \tag{21}$$

and the total collision strength, symmetric in i and j, is given by

$$\Omega_{ij} = \sum_{LS\pi} \Omega_{ij}^{LS\pi} \tag{22}$$

which, for incident energy E$\rightarrow \infty$, behaves like log(E), 1/E^2, and constant for dipole allowed, spin forbidden, and non-dipole allowed transitions, respectively.

The target functions should be such that all the configurations in the complex (the same quantum number and parity) are included; e.g. to calculate 2^1S state of a He-like ion, $2s^2$ and $2p^2$ configurations should be included. We will see below that a large number of configurations are required to obtain a good representation of the bound state wavefunction. Along these lines the program Superstructure (Eissner et al. 1972) developed at UCL takes into account configuration interaction and also includes relativistic corrections using the Breit-Pauli Hamiltonian as a perturbation to the nonrelativistic Hamiltonian. The target functions are expanded in terms of Slater states and the same type of potential $V_i(r)$ as in Equation (16) is used to calculate the radial functions. The potential $V_i(r)$ depends upon parameters λ_l which are determined variationally by optimizing the weighted sum of the term energies. Atomic data such as energy levels, oscillator strengths, and radiative transition rates are calculated in LS and in intermediate coupling. Term coupling coefficients required to transform LS K-matrices to intermediate coupling in the recoupling program JAJOM (Saraph 1978), which calculates collision strengths between the levels, are also calculated in the Superstructure program. Since only a finite number of incident partial waves can be included in the calculation of collision strengths, the contribution from higher partial waves is included using the Coloumb-Bethe approximation (CBe; Burgess and Sheorey 1974) for dipole-allowed transitions and geometric progression for non-dipole allowed transitions. This is referred to as a top-up. The program JAJOM has been modified (Saraph and Eissner 2000) recently to include these contributions in the final results.

Collision strengths have been calculated for a number of ions and before we discuss their applications, we consider one ion, say O III, and illustrate the convergence of collision strengths with the incident partial waves for allowed and forbidden transitions. Energy levels, oscillator strengths, transition rates, and collision strengths for O III have been calculated by using $2s^22p^2$, $2s2p^3$, $2p^4$, $2s^22p3s$, $2s^22p3p$, and $2s^22p3d$ configurations in the Superstrucure and DW programs and they are given by Bhatia and Kastner (1993). These configurations give rise to 46 fine-structure levels. Collision strengths have been calculated at five incident energies (4, 6, 8, 10, and 12 Ry) and up to total angular momentum L^T=21.

$$\vec{L^T} = \vec{l_i} + \vec{l_t} \tag{23}$$

where $\vec{l_i}$ is the incident angular momentum and $\vec{l_t}$ is the target angular momentum. For allowed transitions, we compare in Table 1 some increments in collision strengths, at the highest incident energy 12 Ry, with increasing incident partial wave l_i obtained in the DW calculation and in the CBe approximation. It is seen that for $l_i \geq 19$ the CBe approximation can be used to calculate contributions from higher incident partial waves to collision strengths.

Table 1. Comparison of DW and CBe collision strength increments $\Delta\Omega$ for allowed transitions at incident electron energy=12 Ry.

Transition	$l_i \rightarrow l_i{+}1$	increments $\Delta\Omega$ DW	CBe
$2s^22p^2\ ^3P_0 \rightarrow 2s2p^3\ ^3D_1$	14 15	0.048877	0.048395
	15 16	0.043548	0.043203
	16 17	0.038977	0.038635
	17 18	0.034909	0.034601
$2s^22p^2\ ^3P_0 \rightarrow 2s2p^3\ ^3P_1$	14 15	0.050030	0.049471
	15 16	0.043854	0.043446
	16 17	0.038622	0.038213
	17 18	0.034014	0.033654
$2s^22p3p\ ^3D_2 \rightarrow 2s^23p3d\ ^3F_2$	14 15	2.908503	3.041705
	15 16	2.780783	2.854956
	16 17	2.652672	2.688366
	17 18	2.519384	2.538703

The convergence is quite rapid for the forbidden transitions as indicated in Table 2 and, in general, not many incident partial waves are needed for such transitions. The convergence should be even more rapid for ions ionized more than two times.

Table 2. Comparison of DW and CBe collision strength with increasing number of partial waves l_i for forbidden transitions at incident electron energy=12 Ry

Spin-forbidden Transition	l_i	Ω_{DW}	Spin-allowed Transition	l_i	Ω_{DW}
$2s^22p^2\ ^3P_1 \rightarrow 2s^22p3p\ ^1P_1$	14	0.008192	$2s^22p^2(^3P_0 \rightarrow ^3P_1)$	14	0.080818
	15	0.008196		15	0.080818
	16	0.008199		16	0.080818
	17	0.008202		17	0.080818
	18	0.008204		18	0.080818
$2s^22p^2\ ^1S_0 \rightarrow 2s^22p3p\ ^3D_1$	14	0.001836	$2s^22p^2(^3P_0 \rightarrow ^3P_2)$	14	0.145157
	15	0.001836		15	0.146256
	16	0.001836		16	0.147157
	17	0.001836		17	0.147904
	18	0.001836		18	0.148534

3. Applications

There are a number of electron density sensitive lines emitted from excited states of various ions. This sensitivity is due to the presence of metastable levels among the excited states. In general most of the levels are populated due to excitation from the ground state but a metastable level, e.g. the $^3P_0$ level in Be-like systems, does not decay rapidly by radiative transition and thus can have a substantial population so that the higher levels could be excited from it too. Since the population of the metastable level depends upon electron density, other level populations could also be density sensitive. The critical electron density above which a metastable level population becomes important is given by

$$N_e(critical) = \frac{\sum_i A_{ji}}{\sum_i C_{ji}} \tag{24}$$

where j represents the metastable level and i all other levels to which radiative, collisional excitation, and deexcitation take place.

A number of DW calculations have been carried out on various systems and some comparisons with solar and laboratory observations are available. Line ratios

$$R = \frac{(2s2p\,^3P_2 - 2p^2\,^3P_2)}{(2s^2\,^1S_0 - 2s2p\,^1P_1)} \text{ and } \mathrm{R}^* = \frac{(2\mathrm{s}^2\,^1\mathrm{S}_0 - 2\mathrm{s}2\mathrm{p}\,^3\mathrm{P}_1)}{(2\mathrm{s}^2\,^1\mathrm{S}_0 - 2\mathrm{s}2\mathrm{p}\,^1\mathrm{P}_1)} \tag{25}$$

have been measured in the emission spectra of the Texas experimental tokamak plasma (Huang et al. 1987) for beryllium-like Ti XIX and Sc XVIII for various electron densities, and these ratios agree very well with the DW calculations of Bhatia, Feldman, and Seely (1986). A similar comparison has been made for other beryllium-like ions at electron density of $3.5 \times 10^{13} cm^{-3}$ (cf. Figures 6 and 7 of Huang et al. 1987). A comparison of DW calculations with solar and astrophysical observations is expected to be as good as for the tokamak plasma.

Bhatia, Feldman, and Seely (1986a) give atomic data and spectral line intensities for the beryllium sequence. The atomic data consisting of energy levels, oscillators strengths, transition rates, and collision strengths were calculated using $2s^2$, $2s2p$, $2p^2$, $2s3s, 2s3p, 2s3d, 2p3s, 2p3p$, and $2p3d$ configurations giving rise to 20 fine-structure levels. Proton collisions for the transitions $2s2p(^3P_0$ - $^3P_2)$ and $2s2p(^3P_1$ - $^3P_2)$ have been included using the semiclassical theory of Kastner and Bhatia (1979).

With the DW calculations established as reasonably accurate, results of such calculations are compared with solar observations for a few ions giving emission lines from the visible to the X-ray region. Identifications of optically thin as well as optically thick lines are discussed and wherever possible electron densities in the plasma are inferred from intensity ratios.

4. O IV and Mg VIII

Observations of solar flares on 1973 August 9 and September 7 were obtained by the Naval Research Laboratory's SO82B spectrograph on board Skylab. Since the instruments covered the 960-1600 Å wavelength range, spectra of allowed and intersystem lines of O IV became visible at high electron densities. These lines have been used for density diagnostics. Cook, Keenan, and Bhatia (1994) analyzed these observations using atomic data obtained with the configurations $2s^22p$, $2s2p^2$, and $2p^3$. The intensity ratio of the lines at 1342.99 and 1338.61 Å , due to the transitions $2p^3\,^2D_{3/2} \rightarrow 2s2p^2\,^2P_{3/2,1/2}$, was found not in the ratio of transition rates expected; the lines have the same upper level. This is due to the contamination of H_2 lines at 1342.88 and 1338.57 Å . However, the intensity ratio of the allowed line at 1343.51 Å due to $2p^3\,^2D_{5/2} \rightarrow 2s2p^2\,^2P_{3/2}$ and the intercombination line at 1407.39 Å , due to $2s2p^2\,^4P_{1/2} \rightarrow 2s^22p\,^2P_{3/2}$, was found to be density sensitive, but not temperature sensitive, as shown in Figure 1 of Cook, Keenan, and Bhatia (1994). The observed ratio in the two flares is 0.89 and 0.90 giving an electron density of $1.6 \times 10^{12} cm^{-3}$ at log(T_{max})= 5.2 K, where T_{max} is the temperature of maximum abundance of O IV.

EUV spectral lines of Mg VIII have been observed from the solar corona by Skylab, the Solar EUV Rocket Telescope and Spectrograph (SERTS), and more recently by Solar and Heliospheric Observatory (SOHO). SERTS flights (Thomas and Neupert 1994) in 1989, 1991, and in 1993 measured intensities for lines at 311.78, 313.74, 315.02, 317.01, 339.00, 430.44, and 436.73 Å . All these lines with the exception of 430.44 and 436.73 Å have been measured by SOHO (Harrison et al. 1995) lauched in December 1995. Figure 1 taken from Bhatia and Thomas (1998) shows a comparison of solar active region spectra taken by SERTS-89 and by the Coronal Dignostic Spectrometer (CDS) on SOHO.

Bhatia and Thomas (1998) carried out a calculation using the configurations $2s^22p, 2s2p^2, 2p^3, 2s^23s$, $2s^23p$, and $2s^23d$ in the Superstructure program. These configurations give rise to 20 fine-structure levels. The energy levels, oscillator strengths, and radiative rates have been calculated in intermediate coupling. These are given in Tables 1 and 2 of Bhatia and Thomas (1998). Collision strengths are calculated at five

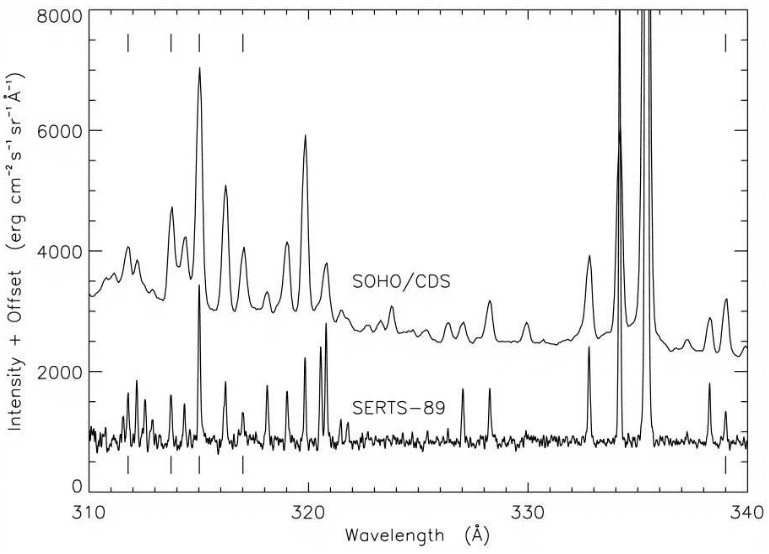

Figure 1. Comparison of average active region spectra taken at different times by SERTS 89 and by CDS on SOHO. The tick marks indicate Mg VIII lines.

incident energies (15.0, 22.5, 30.0, 37.5, and 45 Ry); these are given in Table 2 of Bhatia and Thomas. The temperature of maximum abundance for this ion is $\log(T_e)$=5.9K. Level populations are calculated by solving the statistical equilibrium equations at a number of electron densities, and intensity ratios are then calculated using Equation (1).

A comparison with relative intensities in an active region observed by SERTS-89 is given in Table 3. The calculated intensity ratio I(313.74)/I(317.01)=1.69 agrees reasonably well with the observed value 1.40. The inclusion of 3 more configurations, $2s3p3s, 2s3p3p$, and $2s3p3d$, does not change the above calculated ratio appreciably. These lines originate from the same upper level and therefore the ratio depends only on radiative transition rates. The agreement indicates that the calculated radiative rates are reliable. The relative intensities of 436.73 and 430.44 Å remain in some disagreement with the calculated values. However, the intensity ratio I(436.73)/I(430.44) is found to be density sensitive, and at $N_e = 10^{9.2}$ cm^{-3} (interpolated), its value is 1.68, which is the observed value from SERTS-89 (Thomas and Neupert 1994). This density is comparable to the value of $N_e = 10^{9.6} cm^{-3}$ derived by Brickhouse, Raymond, and Smith (1995) from the same SERTS-89 spectrum, but using Fe IX line ratios formed at temperatures similar to those of Mg VIII.

Atomic data and spectral line intensities for the boron isoelectronic sequence (Ar XIV through Kr XXXII) are given by Bhatia, Feldman, and Seely (1986). The calculations were carried out using $2s^22p$, $2s2p^2$, $2p^3$, $2s^23s$, $2s^23p$, and $2s^23d$ configurations.

5. O III and Fe XXI

Emission lines of carbon-like ions are present in various wavelength ranges, e.g. Fe XXI has emission lines in the ranges 1-25, 90-200, and 300-2500 Å . The Fe ions are of particular interest because Fe is the most abundant element in the solar atmosphere. Many of these lines have been used for electron density diagnostics. Mason et al. (1979) calculated energy levels, oscillator strengths, transition rates, and collision strengths using configurations $2s^22p^2, 2s2p^3$, and $2p^4$ in the Superstructure and DW programs. The levels in the ground configuration $2s^22p^2$ are $^3P_{0,1,2}$, $^1D_2$, and $^1S_0$. Level populations and intensity ratios were calculated at various electron densities and at $T_e = 10^7$ K. The intensity ratios I(142.14)/I(128.73), I(121.22)/I(128.73), I(102.23)/I(128.73), and I(97.89)/I(128.73) are sensitive to N_e as shown in Table 4.

Table 3. Relative intensities observed by SERTS-89 compared to calculated values at $\log(T_e)=5.9$

Transition		λ(Å)	I_{Obs}	I_{cal}				
				log $N_e(cm^{-3})$				
i	j			6	7	8	9	10^c
$2s^22p\ ^2P_{1/2}$	- $2s2p^2\ ^2P_{3/2}$	311.778	$0.313^a \pm 0.056$	0.199	0.199	0.199	0.199	0.199
$2s^22p\ ^2P_{1/2}$	- $2s2p^2\ ^2P_{1/2}$	313.736	0.317 ± 0.049	1.380	1.062	0.540	0.395	0.378
$2s^22p\ ^2P_{3/2}$	- $2s2p^2\ ^2P_{3/2}$	315.024	1.000 ± 0.123	1.000	1.000	1.000	1.000	1.000
$2s^22p\ ^2P_{3/2}$	- $2s2p^2\ ^2P_{1/2}$	317.008	0.227 ± 0.052	0.816	0.628	0.319	0.233	0.223
$2s^22p\ ^2P_{1/2}$	- $2s2p^2\ ^2S_{1/2}$	335.230	—b	0.437	0.357	0.225	0.188	0.184
$2s^22p\ ^2P_{3/2}$	- $2s2p^2\ ^2S_{1/2}$	339.000	0.213 ± 0.033	0.627	0.511	0.322	0.269	0.263
$2s^22p\ ^2P_{1/2}$	- $2s2p^2\ ^2D_{3/2}$	430.445	0.159 ± 0.019	1.614	1.208	0.542	0.356	0.334
$2s^22p\ ^2P_{3/2}$	- $2s2p^2\ ^2D_{5/2}$	436.726	0.267 ± 0.032	0.108	0.255	0.498	0.566	0.574

[a] Blended with Ni XV, see Thomas and Neupert (1994)
[b] Masked by Fe XVI 335.40 Å
[c] Above $\log(N_e)=10$, ratios do not change

Table 4. Theoretical intensity ratios as a function of electron density

λ(Å)	Theoretical intensity ratios for $\log(N_e(cm^{-3}))$						
	11.0	11.5	12.0	12.5	13.0	14.0	15.0
142.14	0.013	0.023	0.055	0.147	0.379	1.246	1.465
128.73	1.000	1.000	1.000	1.000	1.000	1.000	1.000
121.22	0.015	0.044	0.118	0.271	0.538	1.422	1.836
102.23	0.228	0.254	0.321	0.469	0.753	1.720	2.144
97.89	0.099	0.110	0.139	0.204	0.327	0.747	0.930

This sensitivety can easily be understood. Let us consider the lines at 142.14 and 128.73 Å due to the transitions $2s2p^3\ ^3D_2 \rightarrow 2s^22p^2\ ^3P_1$ and $2s2p^3\ ^3D_1 \rightarrow 2s^22p^2\ ^3P_0$, respectively. The level $^3D_2$ is mainly excited from $^3P_1$ while $^3D_1$ is excited from the ground level $^3P_0$. This is because the collision strengths between $^3P_1$ and $^3D_2$ are much larger than between $^3P_0$ and $^3D_2$ as indicated in Table 5.

This implies that at low electron densities most of the population is in the ground level $^3P_0$ as shown in Table 6. Since we are interested mostly in intensity ratios, absolute level populations are not needed. Therefore, N_j in Equation (1) represents fractional level population which is defined as the level population divided by the total population in the ion. The sum of the five fractional level populations is equal to 1.0. As the electron density increases the population of $^3P_1$ increases, the 142.12 line increases in intensity, and therefore the ratio becomes density sensitive.

These calculations were applied to flare spectra obtained from OSO-5. From the I(142.14)/I(128.73) intensity ratios, Mason et al. (1979) concluded that N_e was $<2\times10^{12}cm^{-3}$ in flare B (1969 Feb. 25) and $<5\times10^{12}cm^{-3}$ in flare E (1969 March 12).

Other C-like ions for which atomic data have been calculated are Ne V (Bhatia and Doschek 1993a), Mg VII (Bhatia and Doschek 1995), Si IX (Bhatia and Doschek 1993b), and Ca XV (Bhatia and Doschek 1993c), in addition to OIII (Bhatia and Kastner 1993) as mentioned earlier. The configurations used in the Superstructure and DW programs are $2s^22p^2$, $2s2p^3$, $2p^4$, $2s^22p3s$, $2s^22p3p$, and $2s^22p3d$. This set of configurations give rise to 46 fine-structure levels.

O III is particularly interesting because the He II 303.8 Å resonance line, He II Lyα, coincides with the energy difference between the $2s^22p^2\ ^3P_2$ and $2s^22p3d\ ^3P_2$ levels. Therefore, the He II line photoexcites the $2s^22p3d\ ^3P_2$ from the lower $^3P_2$ level, producing a fluorescent cascade of visible and ultraviolet lines due to the decay of the photoexcited level. This cascade is through the levels of the 2p3p

Table 5. Collision strengths between the levels of 142.14 and 128.73 Å

Transition	Collision strength		
	20 Ry	50 Ry	100 Ry
$^3P_0 \rightarrow ^3D_1$	0.1832	0.2157	0.2520
$^3P_1 \rightarrow ^3D_1$	0.0199	0.0222	0.0248
$^3P_0 \rightarrow ^3D_2$	0.0025	0.0019	0.0013
$^3P_1 \rightarrow ^3D_2$	0.3506	0.4116	0.4784

Table 6. Populations of levels in the ground configurations as a function of electron density[a]

Level	Level population for log(N$_e(cm^{-3})$)=						
	11.0	11.5	12.0	12.5	13.0	14.0	15.0
$^3P_0$	9.67-1	9.06-1	7.75-1	5.80-1	3.77-1	1.45-1	9.84-2
$^3P_1$	7.40-3	2.17-2	5.73-2	1.27-1	2.25-1	3.05-1	2.52-1
$^3P_2$	2.56-2	7.16-2	1.66-1	2.86-1	3.71-1	3.95-1	3.68-1
$^1D_2$	9.72-5	3.86-4	1.73-3	7.44-3	2.65-2	1.42-1	2.45-1
$^1S_0$	5.34-6	1.84-5	6.90-5	2.73-4	1.10-3	1.34-2	3.72-2

[a] Throughout in the tables, a+b=a$\times$10^b

and 2p3s configurations. This is known as the Bowen fluorescence mechanism (Bhatia, Kastner, and Behring 1982). The statistical equilibrium equations are solved in the presence of the He II radiation field to obtain level populations and then intensities of various lines are calculated using Equation (1). A convincing proof of this process comes from the fact that the 303.63 Å line in the spectra of the Sun obtained by Behring et al. (1976) and the multiplet at 644 Å in the Skylab spectra obtained by Vernazza and Reeves (1978) would not have been seen in the absence of this mechanism (see Figure 4 in Bhatia et al. 1982). Also, the calculated intensity of the multiplet at 644 Å in the presence of photoexcitation agrees with the observed intensity. The primary cascade lines (i.e. lines orginating from $2p3d\ ^3P_2$ to the levels of $2p3p$) are 3444.10, 3132.84, 2837.17, and 2819.57 Å and the secondary cascade lines (i.e. lines between the levels of 2p3p and 2p3s) are 3759.87, 3340.75, 3312.30, 3299.36, 3047.13, and 3023.45 Å (Kastner et al. 1983).

There are non-photosensitive multiplets and their calculated intensities agree with the observations: the multiplet components at 508.18 and 703.85 Å agree with the obervations of Behring et al. (1976) and the multiplets at 508, 526, 703, and 835 Å agree with the observations of Vernazza and Reeves (1978).

The ratio I(3444)/I(5007) in planetary nebulae can be used to infer the photoexcitation rate P of the He II resonance line, the 3444 Å line being a Bowen line and the 5007 Å line an optically thin forbidden non-Bowen line. The line at 3444 Å is due to $2s^22p3d\ ^3P_2 \rightarrow 2s^22p3p\ ^3P_2$ and the line at 5007 Å is due to $2s^22p^2(^1D_2 \rightarrow ^3P_2)$. Having established P the electron density can be determined from the density sensitive infrared line ratio I(88.3μm)/I(51.8μm). The line at 88.3 μm is due to $2s^22p^2(^3P_1 \rightarrow ^3P_0)$ and the 51.8μm line due to $2s^22p^2(^3P_2 \rightarrow ^3P_1)$. Since $^3P_2$ is the upper level of the 51.8μm line and the lower level of the pumped transition, the ratio is sensitive to P as well as to N_e which can both be determined by comparing calculated intensity ratios with observations (see Figures 1 and 2 in Bhatia and Kastner 1987).

The O III 374.436 Å line due to $2s^22p3s\ ^3P_1 \rightarrow 2s^22p^2\ ^3P_2$ can photoexcite the N III 374.441 and 374.434 Å lines but a comparison with solar and nebular observations indicates that this process plays a small role, unlike in O III. The quenching of the infrared 57.3 μm line, emitted in the ground configuration transition $2s^22p(^2P_{3/2} \rightarrow ^2P_{1/2})$, is due to photoexcitation from the $2s^22p\ ^2P_{3/2}$ level to

$2s^2 3d\ ^2D_{5/2,3/2}$ levels. This is an indication of the presence of Bowen fluorescence in N III (Kastner and Bhatia 1984).

There are a number of ions for which Bowen fluorescence is possible and Kastner and Bhatia (1986) have suggested a general name of PAR–Photoexcitation by Accidental Resonance. This mechanism can be used to identify the presence of other ions, e.g. in the above case He II.

In the X-ray region, the Fe XXI emission lines in the 9.4 – 9.8 Å range were observed during an intense (GOES class M4.5) flare on 1985 July 2 with the Flat Crystal Spectrometer (FCS) on the Solar Maximum Mission (SMM) satellite (Fawcett et al. 1987). To infer electron density, Phillips et al. (1996) carried out a calculation using configurations $2s^2 2p^2$, $2s2p^3$, $2p^4$, $2s^2 2p4s$, $2s^2 2p4d$, $2s^2 2p5s$, and $2s^2 2p5d$. These configurations give rise to 42 fine-structure levels. The transitions for these X-ray lines along with their wavelengths, oscillator strengths, radiative transition rates, and collision strengths at three incident energies are given in Table 7, where 1, 2, and 3 refer to the levels $^3P_{0,1,2}$ arising from the $2s^2 2p^2$ configuration and 26, 27, 28, 30, and 31 refer to $^1D_2$, $^3F_3$, and $^3D_{1,2,3}$ arising from the $2s^2 2p4d$ configuration. Since the observed wavelengths are accurate to 0.001 Å , 0.049 Å has been added to the calculated wavelengths in order to identify the observed lines.

Table 7. Atomic data for Fe XXI X-ray lines.

Tr.(i-j)	λ(Å)	$\omega_i f_{ij}$	A_{ji}(s^{-1})	Ω(110)	Ω(220)	Ω(330)
1-28	9.476	2.55-1	6.37+12	0.0091	0.0150	0.0187
2-26	9.546	3.30-1	4.88+12	0.0132	0.0202	0.0250
2-28	9.541	4.01-2	9.91+11	0.0028	0.0027	0.0031
2-30	9.457	1.29-1	1.95+12	0.0051	0.0077	0.0095
3-27	9.585	3.50-1	3.67+12	0.0151	0.0215	0.0265
3-31	9.489	5.36-1	5.73+12	0.0201	0.0318	0.0397

A useful relation between the oscillator strength f_{ij} and the transition rate A_{ji} is given by

$$A_{ji} = \frac{6.670 \times 10^{15} \omega_i f_{ij}}{\lambda^2(\AA\,) \omega_j} \tag{26}$$

where ω_i is the weight factor of the level i.

The complete atomic data set obtained for 42 fine-structure levels is used to solve the statistical equilibrium equations. The level populations of the lowest five levels $^3P_{0,1,2}$, $^1D_2$, and $^1S_0$ agree very well with the close-coupling results of Conlon et al. (1992) as indicated in Figure 1 of Phillips et al. (1996). The calculated intensity ratios are compared with the observations in Table 8.

Table 8. Observed and theoretical wavelengths and intensities for Fe XXI

	Observed			Calculated				
		Ident.	Int.		Ident.	Electron Density (cm^{-3})		
Let.	λ(Å)		Ratio	λ(Å)		10^{11}	10^{12}	10^{13}
A	9.455	–	0.080	9.457	2-30	0.003	0.014	0.087
B	9.476	1-28	1.000	9.476	1-28	1.001	1.005	1.032
C	9.482	3-31	0.163	9.489	3-31	0.015	0.088	0.408
D	9.542	2-28	0.138	9.541	2-28	0.155	0.155	0.159
E	9.548	2-30	0.146	9.546	2-26	0.100	0.133	0.370
F	9.587	3-27	0.080	9.585	3-27	0.078	0.127	0.346

The relative intensities of lines C and E are best fitted by a theoretical spectrum with electron density N_e more than 10^{12} cm^{-3} and a comparison of the calculated line spectra with the observed spectrum, given in Figure 5 of Phillips et al. (1996), also indicates a good fit at $N_e = 10^{12} cm^{-3}$.

The fact that the electron density in a flare can be so high is also borne out by Fe XXII lines at 8.976 Å (P) and 9.073 Å (Q and R) observed by the SMM FCS (Fawcett et al. 1987). The line P is due to the transition $2s^24d\ ^2D_{3/2} \rightarrow 2s^22p\ ^2P_{1/2}$, the line Q due to $2s^24d\ ^2D_{5/2} \rightarrow 2s^22p\ ^2P_{3/2}$, and the line R due to $2s^24d\ ^2D_{3/2} \rightarrow 2s^22p\ ^2P_{3/2}$. These lines are not blended with other lines. The observed intensity ratio [I(Q)+I(R)]/I(P)=0.54±0.03. Mason and Storey (1980) carried out a DW calculation and concluded that N_e=$10^{13} cm^{-3}$.

Atomic data and spectral line intensities for the carbon isoelectronic sequence (Ar XIII through Kr XXXI) using $2s^22p^2$, $2s2p^3$, $2p^4$, $2s^22p3s$, $2s^22p3p$, and $2s^22p3d$ configurations are given by Bhatia, Seely, and Feldman (1987).

6. Mg VI

Eight lines of Mg VI in the EUV range have been identified in the SERTS-89 data (Thomas and Neupert 1994). To identify these lines and also X-ray lines observed earlier by Behring et al. (1972), Bhatia and Young (1998) extended the earlier calculations of Bhatia and Mason (1980) who dealt with Mg VI, Si VIII, S X, Ar XII, and Ca XIV, by adding another configuration $2s^22p^23s$ to the configurations $2s^22p^3$, $2s2p^4$, and $2p^5$. Collision strengths are calculated at five incident energies, 7, 10, 35, 50, and 85 Ry, and for incident partial waves up to 19. Proton rates within five levels, $^4S_{3/2}$, $^2D_{3/2,5/2}$ and $^2P_{1/2,3/2}$, of the $2s^22p^3$ configuration have been included in the calculation of intensities for N_e=10^8, 10^{10}, and 10^{12} cm^{-3} and log(T_e)=5.45, 5.60, and 5.75K.

This model predicts lines at 387.77, 387.93, and 388.00 Å . Since the 388.00 Å line is the most intense of these three, the line observed at 387.955 Å is identified with the predicted 388.00 Å line due to $2s2p^4\ ^2D_{1/2} \rightarrow 2s^22p^3\ ^2P_{3/2}$. The line observed at 349.162 Å is identified as a blend of the four predicted lines at 349.11, 349.12, 349.16, and 349.18 Å . Similarly, the observed line at 270.401 Å is identified with a blend of 270.39 and 270.40 Å . The observed intensity ratio of the lines 399.275 and 403.296 Å agrees with the predicted intensity ratio.

The observed X-ray lines (Behring et al. 1972) are 111.557 and 111.724 Å , 111.557 Å being the stronger of the two, in agreement with the calculations.

Atomic data for Ne IV have been calculated by Bhatia and Kastner (1988) by including configurations $2s^22p^3$, $2s2p^4$, $2p^5$, $2s^22p^23s$, $2s^22p^23p$, and $2s^22p^23d$. These configurations give rise to 72 fine-structure levels. The multiplets at 358.7, 421.6, and 469.8 Å are found to be density sensitive at log($N_e(cm^{-3})$)= 6 to 12 (see Figure 5 in Bhatia and Kastner 1988). The PAR process (Kastner and Bhatia 1986) mentioned above is possible in this ion because of excitation by a coincident wavelength of Fe XI.

Atomic data and spectral line intensities for the nitrogen isoelectronic sequence (Ar XII through Kr XXX) are given by Bhatia, Seely, and Feldman (1989). The calculations were carried out by including the configurations $2s^22p^3, 2s2p^4, 2p^5, 2s^22p^23s, 2s^22p^23p$, and $2s^22p^23d$. This set of configurations gives rise to 72 fine-structure levels.

7. Fe XVII and resonance scattering

Neon-like Fe XVII is present in flares and solar active regions in a broad temperature range (2-10)×10^6 K because of the filled 2p shell. Strong resonance lines in the range 15-17 Å have been observed by McKenzie et al. (1980) and Phillips et al. (1982). The transitions of interest are $2s^22p^53d\ ^1P_1 \rightarrow 2s^22p^6\ ^1S_0$ at 15.02 Å and $2s^22p^53d\ ^3D_1 \rightarrow 2s^22p^6\ ^1S_0$ at 15.26 Å along with subordinate lines in the extreme-ultraviolet (EUV) region.

There have been a number of theoretical studies of the expected spectrum assuming optically thin conditions. Bhatia and Doschek (1992) carried out a DW calculation using seven configurations, $2s^22p^6$, $2s^22p^53s$, $2s^22p^53p$, $2s^22p^53d$, $2s2p^63s$, $2s2p^63p$, and $2s2p^63d$, giving rise to 37 fine-structure levels. Collision strengths were calculated at five incident energies: 76.83, 91.53, 120.93, 179.73, and 253.23 Ry. Their collision strengths are in good agreement with those of Zhang et al. (1987), Zhang and Sampson (1989), and Hagelstein and Jung (1987). The level populations and intensity ratios were calculated as a function of electron density and temperature.

The Fe XVII level structure is distinguished in having all the excited levels much higher than the single ground level $^1S_0$, implying that even at high electron densities most of the ion population is in the ground level. The EUV lines have been observed in solar flare spectra recorded by a Naval Research Laboratory slitless spectrograph flown on the Skylab manned space station in 1973 (Feldman et al. 1985; Doschek, Feldman and Bhatia 1991). The predicted relative intensities of these lines at N_e=10^{11} cm^{-3} and T_e=4×10^6K agree fairly well with the observed relative intensities, which are accurate to within 30%.

For optically thin plasma, the ratio I(15.02)/I(15.26) according to the calculation is 4.8, while the observed (McKenzie et al. 1980; Phillips et al. 1982) ratio is 2.75 $\pm$ 0.7 and the experimental value of Brown et al. (1998) using Electron Beam Ion Trap (EBIT) is 3.04 $\pm$ 0.12. The observed intensity ratios of various lines do not agree with the optically thin calculated intensity ratios and it is clear that these lines suffer resonance scattering as suggested by Rugge and McKenzie (1985). Resonance scattering implies that the emitted photon is absorbed and reemitted but not necessarily in the line of sight, so, there can be an apparent loss of flux although the total flux integrated over 4π remains unchanged.

The optical depth at the line center is given by

$$\tau_0 = \int k_0 dl = \frac{\pi e^2}{m_e c} f (N_1 L) \phi(\nu) \tag{27}$$

where k_0 is the absorption coefficient, f the oscillator strength, $N_1(cm^{-3})$ the population of the ground state, $L(cm)$ the path length; neglecting nonthermal velocities, the Gaussian line profile function at the line center is

$$\phi(\nu) = \lambda(cm)\sqrt{\frac{m_{ion}}{2\pi k T_{ion}}} = \frac{1}{\sqrt{\pi}\Delta\nu_{thin}} = \frac{1}{\sqrt{\pi}\Delta\nu_D} \tag{28}$$

where m_{ion} is the ion mass in amu units and T_{ion} is the ion temperature which can be taken equal to T_e.

$$\tau_0 = \frac{\sqrt{\pi}e^2}{m_e c} f\lambda\sqrt{\frac{m_{ion}}{2kT_e}}(N_1 L) \tag{29}$$

$N_1 L(cm^{-2})$ is the column length, which can be taken out of the integral for the uniform case. It can be shown that

$$\tau_0 = 1.161 \times 10^{-14} f\lambda(\text{Å})\sqrt{\frac{M}{T_e}}(N_1 L) \tag{30}$$

It should be noted that τ_0 is a function of electron temperature and M is the atomic mass number. For T_e=4×10^6K and M=56 for Fe, we find

$$\frac{\tau_0}{(N_1 L)} = 4.35 \times 10^{-17} f\lambda \tag{31}$$

Table 9 from Table 3 of Bhatia and Kastner (1999) gives λ, f, A, and $\tau_0/N_1 L$ for transitions originating from the $3s$, $3p$, and $3d$ levels at $T_e = 4 \times 10^6$ K.

The forbidden magnetic quadrupole line $2p^5 3s(^3P_2) \rightarrow 2p^6(^1S_0)$ at 17.10 Å has been included because it can be intense due to overpopulation of the $^3P_2$ level. It is seen from the table that the 15.02 Å line has $\tau_0 \simeq 2$ for $N_1 L = 10^{15} cm^{-2}$ due to the large oscillator strength, and therefore can suffer resonance scattering, i.e. loss of flux.

The simplest way to take into account optical depth effects is to multiply the transition rates by constant escape probabilities. Various approximate treatments, e.g. Phillips et al. (1996) and Saba et al. (1999) have been carried out to interpret observations of the disk center to limb intensity variation. Saba et al. used the escape probability method of Kastner and Kastner (1990) and concluded that the intensity of the 15.02 Å line is a factor of 2 to 3 lower than the predicted optically thin value. It is very unlikely that other processes like dielectronic recombination, inner-shell ionization, polarization of lines, etc. will remove the discrepancy between observations and calculations.

These studies indicate that the strongest line at 15.02 Å can have significant optical depth in solar active regions and in flares.

Table 9. Fe XVII Resonance lines and forbidden line 17.10 Å

Upper Level[a]	λ(Å)	f	$A(s^{-1})$	τ_0/N_1L
$2p^5 3s\ ^3P_2$	17.10	4-8	1.69+5	0.0
$2p^5 3s\ ^1P_1$	17.05	0.123	9.44+11	7.50-17
$2p^5 3s\ ^3P_1$	16.78	0.101	8.00+11	8.98-17
$2p^5 3d\ ^3P_1$	15.45	0.089	8.27+10	5.96-18
$2p^5 3d\ ^3D_1$	15.26	0.593	5.69+12	3.94-16
$2p^5 3d\ ^1P_1$	15.02	2.662	2.64+13	1.74-15
$2s2p^6 3p\ ^1P_1$	13.82	0.275	3.21+12	1.66-16

[a] Lower level is ground level $2p^6\ ^1S_0$.

Recently, Bhatia and Kastner (1999) solved Equation (2) for $T_e = 4\times10^6$K and $N_e = 10^{11}\ cm^{-3}$ iteratively by multiplying transition rates by escape factors appropriate to the chosen geometry and emergent intensities by monodirectional escape probabilities.

The Doppler-profile escape factor for slab geometry has been given by Capriotti (1965) as

$$SEF(\tau) = 1 - (0.8293)\tau + (0.7071)\tau ln(2\tau) + \sum_{k=1}^{\infty} \frac{(-1)^k (2\tau)^{2k+1}}{k(k+2)!(k+2)^{1/2}} \tag{32}$$

for $\tau \leq 2.5$, and

$$SEF(\tau) = \frac{((ln(2\tau))^{1/2} + 0.25(ln(2\tau))^{-1/2} + 0.14)}{(2\sqrt{\pi}\tau)} \tag{33}$$

for $\tau > 2.5$. The monodirectional single-flight or free-flight photon escape probability, assuming a constant source function, is given by (Kastner and Kastner 1990) as

$$p_f(D, \tau; 1) = (\sqrt{\pi}\tau)^{-1} \int_{-\infty}^{\infty} (1 - \exp(-\tau \exp(-x^2)))dx \tag{34}$$

where the dimensionless frequency variable $x = (\nu - \nu_0)/\Delta\nu_D$. The escape probability, expressed as a logistic function, is given by

$$p_f(D, \tau; 1) = \frac{1}{1 + \exp(b(log(\tau) - c))} \tag{35}$$

where b=2.410527 and c=0.3950445. The present analysis is valid for lines which are not self-reversed, i.e. $0 < \tau < 10$. Similar expressions are given for cylindrical geometry by Bhatia and Kastner (1999) and in this case b=2.3212136 and c=0.22335545 in expression (35). The emergent intensity for an optically thick plasma is decreased from the optically thin value and is now given by

$$I_{ji} = N_j A_{ji} \Delta E_{ij} p_f(D, \tau; 1) = I_{ji}(\text{optically thin})\mathrm{p_f(D}, \tau; 1) \tag{36}$$

Equation (2) becomes nonlinear (see Equations (1) and (2) in Bhatia and Kastner 1992) in level populations when the optical depth effects are included and then the equations have to be solved non-iteratively or by the Newton-Raphson method (Bhatia and Kastner 1992). Both the methods give the same results. It is found that the upper level populations of the resonance lines increase with the column length; variation of the upper level $2p^5 3d\ ^1P_1$ of the most optically thick resonance line at 15.02 Å at T_e=4$\times$10^6 K and for N_e=10^9, 10^{10}, and 10^{11} cm^{-3} is shown in Figure 2 taken from Bhatia and Kastner (1999).

The level population increases by a factor of 1000 at a column length of $10^{21}\ cm^{-2}$ compared to its optically thin value.

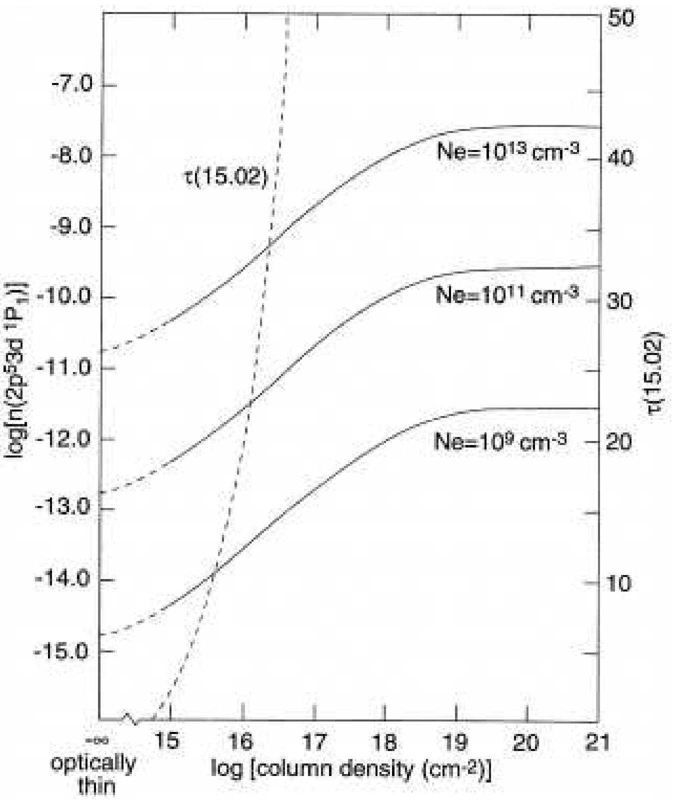

Figure 2. Variation of the population of the upper level $2p^5 3d(^1P_1)$ of the 15.02 Å resonance line, with increasing column density of Fe XVII.

The calculated photon fluxes of the six resonance lines listed in Table 9 relative to the reference line at 17.10 Å are given in Table 10 for active regions (T_e=4×10^6 K and N_e=10^{11} cm^{-3}) for the plane-parallel (slab) geometry.

Similar tables are given in (Bhatia and Kastner 1999) for flare temperatures and cylindrical geometry. It is seen from Table 10 that all resonance lines show an initial increase in flux relative to the forbidden line as the column density increases. Also, intensities of the 15.02 and 15.26 Å lines with respect to the 16.78 Å line, due to $2p^5 3s\ ^3\mathrm{P}_1 \rightarrow 2p^6\ ^1S_0$, first increase with column density and then decrease (see Figures 3 and 4 from Bhatia and Kastner 1999), contrary to conventional wisdom which holds that the intensities of resonance lines always decrease with an increase of optical depth. This should be relevant for interpretation of future observations.

As expected, all the EUV lines originating from 3d levels are also affected by the opacity as indicated in Table 11 (for T_e=4×10^6 K and N_e=10^{11} cm^{-3}; see also Figure 4 of Bhatia and Kastner 1999). Eleven lines at 193.7, 226.1, 240.4, 243.0, 295.98, 324.5, 340.1, 351.6, 358.24, 373.41, and 387.23 Å increase in intensity with respect to the 254.9 Å line with an increase in column length, reaching saturation values at a column length of 10^{21} cm^{-2}. The magnetic dipole transition $2p^5 3s(^3P_0$ - $^1P_1)$ at 1153.2 Å is also enhanced by opacity.

Wood and Raymond (2000), using a 3D Monte Carlo radiation transfer code, have investigated the effects of resonance scattering of emission lines on the emergent fluxes from coronal loop structures. They find, depending on viewing angle, the emergent flux may be lower or higher than the optically thin prediction due to scattering out of or into the line of sight.

For a source which is uniform over the field of view and along the line of sight, an estimate of the electron density can be made from the decrease in the flux of the resonance line (Schmelz et al. 1992).

Table 10. X-ray photon flux ratios[a] in slab geometry.

$\log(N_1\mathrm{L(cm^{-2})})$	17.05	16.78	15.45	15.26	15.02	13.82
$-\infty$	0.176	0.0992	-0.933	-0.157	0.453	-1.086
13	0.177	0.100	-0.933	-0.153	0.465	-1.085
14	0.183	0.105	-0.932	-0.135	0.514	-1.076
15	0.216	0.134	-0.929	-0.0563	0.654	-1.032
16	0.336	0.243	-0.911	+0.0811	0.713	-0.921
17	0.473	0.378	-0.852	0.0698	0.689	-1.044
18	0.597	0.465	-0.958	-0.147	0.466	-1.652
19	0.712	0.551	-1.589	-0.808	-0.169	-2.572
20	0.727	0.561	-2.461	-1.705	-1.069	-3.517
21	0.733	0.566	-3.406	-2.657	-2.066	$<$ -4

[a] Entries are $\log[\mathrm{F}(\lambda)/\mathrm{F}(17.10)]$; column headings are line wavelengths (Å)

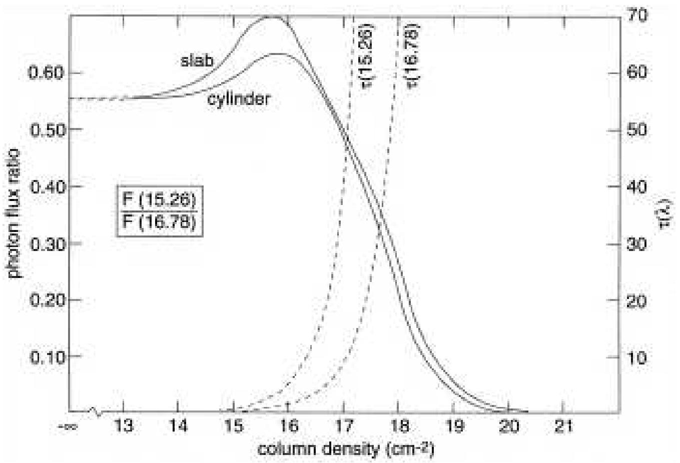

Figure 3. Column density dependence of the the 15.02 Å resonance line photon flux in slab and cylindrical geometry, relative the flux of the 16.78 Å line.

The number density can be written as

$$N_1 = \frac{N_1}{N(FeXVII)}\frac{N(FeXVII)}{N(Fe)}\frac{N(Fe)}{N(H)}\frac{N(H)}{N_e}N_e \tag{37}$$

Since most of the population is in the ground state, $N_1/N(FeXVII) = 1$; taking $N(FeXVII)/N(Fe) =$ 0.776 (Arnaud and Rothenflug 1985), $N(Fe)/N(H)$=10^{-4} (which is 4 times the photospheric abundance; Feldman 1992), and $N(H)/N_e = 0.8$ in regions where hydrogen is mostly ionized, Equation (37) gives

$$N_1 = 0.6208 \times 10^{-4} N_e \tag{38}$$

Using Equation (31), we have for the 15.02 Å line

$$\tau_0 = 1.080 \times 10^{-19} N_e L = 1.080 \times 10^{-19}\frac{EM}{N_e} \tag{39}$$

where the column emission measure EM is defined as

$$EM = \int N_e^2 dl \tag{40}$$

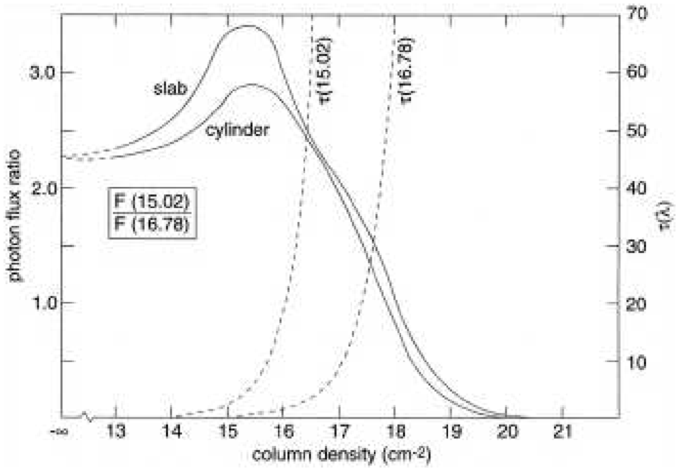

Figure 4. Column density dependence of the the 15.26 Å resonance line photon flux in slab and cylindrical geometry, relative the flux of the 16.78 Å line.

From Schmelz et al. (1992), for NOAA active region 4891, log(EM)=29.17. This gives

$$\tau_0 = 1.598 \times 10^{10}/N_e \qquad (41)$$

A flux decrease of a factor of 2 implies that the monodirectional escape probability=0.5 which from Kastner and Kastner (1990) or Equation (35) means τ_0=2.512. This gives $N_e = 6.36 \times 10^9 cm^{-3}$, a plausible value for the electron density.

We considered here only monodirectional escape probability $p_f(D, \tau; 1)$ from a unformly emitting source (homogeneous) while there is a corresponding escape probability $p_f(D, \tau; 0)$ for a source in which emitting and absorbing ions are spatially separated (inhomogeneous), see Kastner and Kastner (1990) for more details.

Even though I(15.02)/I(17.10) and I(15.02)/I(17.05) are sensitive to electron temperature they cannot be used for temperature diagnostics because of the resonance scattering of the 15.02 Å line. Instead, Fe XVII X-ray lines in conjunction with Fe XVIII lines have been used for temperature diagnostics (Phillips et al. 1997). The relative abundance of Fe XVII to Fe XVIII required in the intensity ratio for temperature diagnostics (see Equations (2) and (8) in Phillips et al. 1997) is known. The intensity ratio of the strong Fe XVIII line at 16.073 Å due to $2p^4 3s\ ^4P_{5/2} \rightarrow 2p^5\ ^2P_{3/2}$ to the Fe XVII 16.773 Å line is sensitive to T_e as indicated in Figure 5 of Phillips et al.

An unidentified line in the solar spectra of Parkinson (1975) was identified by Bhatia and Kastner (1985) as the electric quadrupole line at $2s^2 2p^5 3p\ ^3P_2 \rightarrow 2s^2 2p^6\ ^1S_0$ at 16.33 Å in Fe XVII; this has been confirmed by Brown et al. (1998).

Atomic data and spectral line intensities for the neon isoelectronic sequence (Si V through Kr XXVII) are given by Bhatia, Feldman and Seely (1986b). The calculations included configurations $2s^2 2p^6, 2s^2 2p^5 3s, 2s^2 2p^5 3p$, and $2s^2 2p^5 3d$. These configurations give rise to 27 fine-structure levels.

8. Fe XV

Fe XV is of interest because X-ray lines in the range 53.07 to 73.94 Å from an M-class solar flare have been observed by Acton et al. (1985) with a high-resolution rocket-borne grazing incidence spectrograph telescope (XSST). Bhatia, Mason, and Blancard (1997) carried out a DW calculation using configurations $3s^2, 3s3p, 3p^2, 3s3d, 3p3d, 3s4s, 3s4p, 3s4d, 3s4f, 3p4s, 3p4p, 3p4d$, and $3p4f$, giving rise to 78 fine-structure levels. Energy levels, transition rates, and collision strengths at incident electron energies of 25, 50, and 75 Ry were calculated and statistical equilibrium equations were solved for level

Table 11. Relative intensities[a] of EUV lines enhanced by opacity[b].

λ(Å)	-∞	16	17	18	19	20
193.7	<-4.0	-2.143	-1.219	-0.532	-0.276	-0.288
226.1	<-4.0	-1.785	-0.929	-0.232	+0.045	+0.092
240.4	<-4.0	-2.051	-1.127	-0.441	-0.217	-0.196
243.0	<-4.0	-2.193	-1.342	-0.663	-0.407	-0.419
296.0	-0.982	-0.965	-0.854	-0.560	-0.383	-0.395
324.5	<-4.0	-2.180	-1.256	-0.570	-0.313	-0.325
340.1	-1.038	-1.022	-0.915	-0.631	-0.428	-0.469
351.6	-1.293	-1.276	-1.170	-0.886	-0.712	-0.724
358.2	-0.905	-0.880	-0.733	-0.397	-0.290	-0.221
373.41	-1.235	-1.204	-1.017	-0.617	-0.438	-0.421
387.2	-1.138	-1.107	-0.920	-0.520	-0.341	-0.324
1154	-1.346	-1.325	-1.22	-0.865	-0.758	-0.689

[a] Entries are log[F(λ)/F(254.9)]; column headings are log(column density)(cm^{-2})
[b] Cylindrical geometry

populations to calculate intensity ratios at N_e=10^8, 10^9, 10^{10}, 10^{11}, and 10^{12} cm^{-3} and log(T_e)=6.7K. Results for four transitions are given in Table 12.

Table 12. Collision strengths and intensity ratios for a few transitions in Fe XV.

Transition	Collision Strengths			Intensity
	25	50	75(Ry)	log T_e=6.7
3s^2 ^{1}S$_0$ - 3s4s ^{3}S$_0$	2.169-3	8.830-4	4.730-4	
3s^2 ^{1}S$_0$ - 3s4s ^{1}S$_0$	9.506-2	1.054-1	1.088-1	
3s4s ^{1}S$_0$ - 3s3p ^{1}P$_1$	1.739-2	3.646-2	5.179-2	3.88
3s^2 ^{1}S$_0$ - 3s4p ^{1}P$_1$	1.052-2	2.786-2	4.457-2	1.00

This calculation shows that the collision strengths for the monopole transition $3s^2\ ^1S_0$ to $3s4s\ ^1S_0$ are very large. This results in appreciable intensity of the dipole-allowed line $3s4s\ ^1S_0$ to $3s3p\ ^1P_1$ at 69.74 Å , consistent with the observed intensity of the unidentified line at 69.644 Å .

The emission lines in Fe XV have also been observed by SERTS in an active region on the Sun. The 13-configuration calculation of Bhatia, Mason, and Blancard (1997) did not include $3d^2$ which resulted in a poor representation of the $3p^2\ ^1S_0$ level. Therefore, Bhatia and Mason (1997) calculated atomic data using configurations $3s^2, 3s3p, 3p^2, 3s3d, 3p3d$, and $3d^2$. Recently, Eissner et al. (1999) have carried out an R-matrix calculation using exactly the same set of configurations. The two calculations agree so far as the energy levels and transition rates are concerned because the same set of configurations was used in the Superstructure program. A comparison between collision strengths at 50 Ry, obtained in the DW approximation and R-matrix approach, for a few transitions chosen at random indicated in Table 13, shows that DW results are reliable.

The inclusion of resonances will certainly not give the same rate coefficients. But it is known that at high temperatures the contribution of resonances becomes less important and it can be seen in Figure 5 (taken from Eissner et al. 1999) that the effective collision strengths are not too different at the temperature of maximum abundance (log(T_e) = 6.4K) of Fe XV compared to the DW results.

The level populations obtained using the DW and R-matrix rates agree very well. Using the DW atomic data, we calculated the intensity ratios of various extreme-ultraviolet (EUV) lines in Fe XV at N_e=10^{11}, 10^{12}, and 10^{13} cm^{-3} and compare them with those observed in active regions of the Sun by SERTS in Table 14.

Table 13. Comparison of collision strengths in Fe XV from DW and R-matrix calculations.

Transition	Bhatia and Mason	Eissner et al.
$3s^2\ ^1S_0$ - $3s3p\ ^1P_1$	4.135	4.176
$3s3p\ ^3P_0$ - $3s3d\ ^3D_1$	1.171	1.164
$3s3p\ ^3P_1$ - $3p^2\ ^3P_2$	1.566	1.551
$3s3p\ ^3P_2$ - $3s3d\ ^3D_3$	5.015	4.976
$3s3p\ ^1P_1$ - $3p^2\ ^1S_0$	1.961	1.910

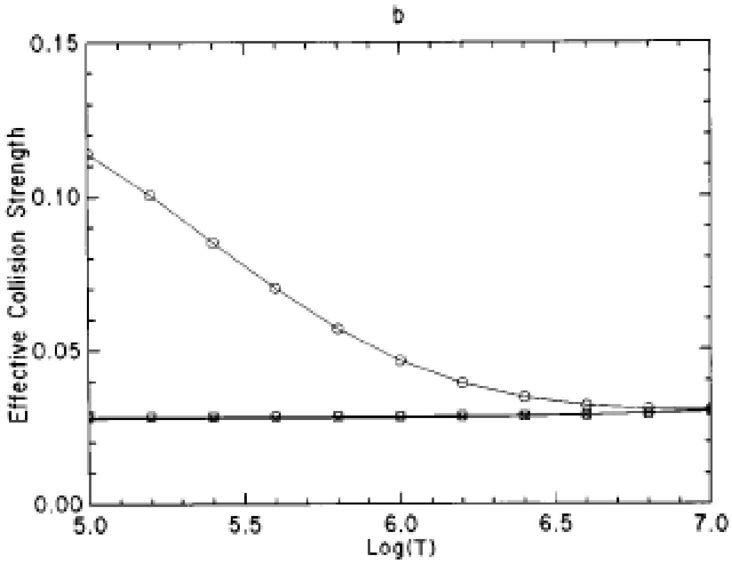

Figure 5. Comparison of the R-matrix (upper curve) and DW (lower curve) effective collision strengths of Fe XV vs. temperature.

The lines at 292.251 and 321.782 Å indicate a density of $N_e = 10^{11}$ cm^{-3}. It should be noted that, although Thomas and Neupert (1994) identified the 292.251 Å line as Si X, Young et al. (1998) have recently ascribed it to the Fe XV transition used in our analysis. The agreement with electron density we find using other Fe XV lines would tend to confirm this later identification.

9. Fe X

There are three famous lines: "green line" at 5303 Å in Fe XIV, "yellow line" at 5694 Å in CA XV, and "red line" at 6374 Å in Fe X in the Sun. The latter is a visible forbidden line in the ground configuration $3s^2 3p^5$ due to the transition $^2P_{1/2} \rightarrow ^2P_{3/2}$. Edlén, comparing such lines in the solar spectra to the laboratory spark spectra, concluded that the temperature of the solar corona is of the order of a million degrees. Strong EUV lines of Fe X have been observed in the solar spectrum of the full Sun obtained by Malinovsky and Heroux (1973) during a sounding rocket flight. Thomas and Neupert (1994) identified lines at 257.26 and 345.72 Å as Fe X lines in SERTS-89 flight. The most recent observations are the lines at 174.526, 175.265, 177.240, 184.534, 190.046, 220.862, and 257.246 Å from the SERTS-95 (Brosius et al. 1998), and with improved calibration of the lines at 174.5338 and 177.2477 Å (Brosius et al. 1999).

Bhatia and Doschek (1995a) calculated atomic data using $3s^2 3p^5$, $3s3p^6$, $3s^2 3p^4 3d$, and $3s3p^5 3d$ configurations in the SUPERSTRUCTURE and DW programs. These configurations give rise to 54 fine-

Table 14. Comparison of calculated intensities at log(T_e)=6.4K with observations[a].

Transition	λ(Å)	Observed	log N_e(cm^{-3}) 11	12	13
3s3d $^1D_2$ - 3s3p $^1P_1$	243.780	7.21-2	4.79-2	4.79-2	4.79-2
3s3p $^1P_1$ - 3s^2 $^1S_0$	284.158	1.000	1.000	1.000	1.000
3p^2 $^3P_2$ - 3s3p $^3P_1$	292.251	5.78-3	6.85-3	7.37-3	7.44-3
3p^2 $^3P_1$ - 3s3p $^3P_2$	321.782	4.68-3	5.11-3	5.53-3	5.59-3
3p^2 $^1D_2$ - 3s3p $^3P_2$	327.030	1.16-2	9.95-3	1.01-2	1.01-2
3s3d $^3F_4$ - 3s3d $^3D_3$	372.758	2.14-2	1.01-3	1.10-3	1.11-3
3s3p $^3P_1$ - 3s^2 $^1S_0$	417.245	4.48-2	2.59-2	2.58-2	2.75-2

[a]Thomas and Neupert, ApJ Suppl. **91**, 461 (1994)

structure levels. Collision strengths were calculated at five incident energies (9, 18, 27, 36, and 45 Ry) and up to the total angular momentum L^T=21. They calculated level populations (at log($N_e(cm^{-3})$)= 8-12 and log(T_e) =6K) and intensity ratios of various lines by including proton impact excitation rates and solar background radiation.

They suggested that the four unidentified lines at 220.86, 238.71, 257.26, and 324.71 Å in the representative spectra in the atlas published by Feldman et al. (1987) as Fe X lines. A number of UV forbidden lines in the range 1000 to 3000 Å have been observed in solar spectra. In the line list published by Feldman and Doschek (1977a), the lines at 1582.60, 1603.31, 1611.7, and 1918.27 Å have been identified as Fe X lines. These identifications have been further confirmed by Bhatia and Doschek as Fe X lines from the intensity ratios they calculated.

The line at 257.26 Å is a blend of two lines from the transitions $3p^4 3d(^4D_{7/2,5/2} \rightarrow ^2P_{3/2})$ and the ΔJ=2 transition is a magnetic quadrupole transition. Therefore, the $^4D_{7/2}$ level can get much more populated than the $^4D_{5/2}$ level as indicated in Table 15 which gives level populations of the lowest five levels. This is a good example of a metastable level mentioned earlier.

Table 15. Level populations of the lowest five levels in Fe X.

configuration	Density / Level	10^8	10^9	10^{10} Population	10^{11}	10^{12}
$3s^2 3p^5$	$^2P_{3/2}$	0.983+00	0.912+00	0.708+00	0.600+00	0.585+00
	$^2P_{1/2}$	0.113-01	0.435-01	0.152+00	0.216+00	0.226+00
$3s3p^6$	$^2S_{1/2}$	0.213-10	0.205-09	0.187-08	0.179-07	0.178-06
	$^4D_{5/2}$	0.127-07	0.137-06	0.146-05	0.124-04	0.115-03
	$^4D_{7/2}$	0.106-02	0.843-02	0.289-01	0.318-01	0.295-01

These calculations did not included the resonance contribution. Young et al. (1996), including the resonance contribution for the ground transition $^2P_{3/2} \rightarrow {^2P_{1/2}}$ from Pellan and Berrington (1995) in the above data, calculated the I(257.26)/I(354.72) ratio at various N_e. Comparing to the observed ratio 1.2 (subflare) and 2.5 (active region loops) in the SERTS-89 spectra, they concluded that N_e=2.5×10^{10} and 2.0×10^9 cm^{-3} for the subflare and active region loops, respectively.

10. Fe VIII

A number of Fe VIII spectral lines in the range 130 to 190 Å have been observed under quiet solar conditions by a grazing-incidence spectrograph with a spectral resolution of 0.06 Å flown on Aerobee-200 rockets (Behring et al. 1972, 1976). The lines at 185.221 and 187.247 Å have been observed from

SERTS-95 flight (Brosius et al. 1998), the former is blended with a Ni XVI line. The same line has also been observed with the RES-K spectrograph on board KORONAS-I satellite (Zhitnik et al. 1998). Bhatia and Eissner (2000) have calculated atomic data using configurations $3p^63d, 3p^53d^2, 3p^64s, 3p^64p$, and $3p^63d4s$. These configurations give rise to 73 fine-structure levels. Collision strengths are calculated at 10, 30, 50, 70 Ry and for the total angular momentum L^T up to 33.

The level populations and intensities of various lines have been calculated at $\log(N_e(cm^{-3}))$=8-14 and $\log(T_e)$=5.57K. It is found that the forbidden infrared 5.447 μm line is a density insensitive line and is due to the transition $3p^63d(^2D_{5/2} \rightarrow {}^2D_{3/2})$. This line should be useful to determine properties of coronal magnetic fields by measuring the Zeeman effect or Faraday rotation. Such infrared lines are called coronal lines because they originate in the ground levels of ions produced at very high, i.e. coronal, temperatures.

The observed lines at 168.170 and 168.546 Å are due to the transitions $3p^53d^2\ {}^2D_{5/2} \rightarrow 3p^63d\ {}^2D_{5/2}$ and $3p^53d^2\ {}^2P_{3/2} \rightarrow 3p^63d\ {}^2D_{5/2}$ and their observed intensity ratio is 12/7=1.7 which agrees well with the calculated ratio 0.0991/0.0527=1.9 at N_e=10^8 cm^{-3}. The observed line at 168.929 Å due to the transition $3p^53d^2\ {}^2P_{1/2} \rightarrow 3p^63d\ {}^2D_{3/2}$ has intensity comparable to that of the line at 168.546 Å but appears to be blended with a 2nd order line at 84.491 Å . The calculated intensity at N_e=10^8 cm^{-3} is 0.035 which is less than the calculated value 0.0527 of the 168.546 Å line, in agreement with the observations that the line is blended. These line ratios are not sensitive to electron densities.

The lines at 159.705, 168.929, 186.599, and 256.981 Å with respect to the line at 168.173 Å are sensitive to electron density in the range $\log(N_e\ (cm^{-3}))$=8 to 10. The intensity ratio of the lines at 195.972 and 194.661 Å is sensitive to electron density in the same range.

11. Determination of T$_e$

So far it has been assumed that T_e is known from the ionization balance. It is also possible to infer electron temperatures from temperature-sensitive allowed lines when they are observed for the same ion and do not differ too much in wavelength (to avoid large calibration uncertainties). Such lines, for example, are present in Mg II. Indicating $3s, 3p$, and $3d$ levels by 1, 2, and 3, the intensity ratio of two emission lines from $3d \rightarrow 3p$ and $3p \rightarrow 3s$ in the absence of chromospheric radiation can be written as

$$\frac{I_{32}}{I_{21}} = \frac{\Delta E_{13} C_{13}}{\Delta E_{12} C_{12}} \propto \exp(\frac{\Delta E_{12} - \Delta E_{13}}{kT_e}) \tag{42}$$

Since $\Delta E_{13} \approx 2\times\Delta E_{12}$ the ratio is sensitive to T_e. Feldman and Doschek (1977b) analyzed the Mg II spectra recorded by the NRL normal-incidence slit spectrograph on Skylab. These lines are emitted around 2800 Å within a few Å of each other. A comparison with observations indicates $T_e \leq 1.8\times10^4$K in the quiet Sun and active regions. This is in agreement with the predicted temperature of formation of Mg II based on the ionization equilibrium calculation of Jordan (1969).

Also, the intensity ratio of a satellite line formed due to dielectronic recombination to the allowed line can be used for temperature determination (Doschek 1985). The allowed line w($1s2p\ {}^1P_1 \rightarrow 1s^2\ {}^1S_0$) is due to electron impact excitation of $1s^2\ {}^1S_0$ in He-like ions and the line j($1s2p^2\ {}^2D_{5/2} \rightarrow 1s^22p\ {}^2P_{3/2}$) is a satellite line formed due to dielectronic recombination of an electron with a He-like ion:

$$e^- + X(1s^2(^1S_0)) \rightarrow X(1s2p^2(^2D_{5/2})) \rightarrow X(1s^22p(^2P_{3/2})) + h\nu \tag{43}$$

The electron impact excitation of $^2D_{5/2}$ from the ground levels is not significant for Li-like ions. The intensity ratio is given by

$$\frac{I_j}{I_w} = \beta\frac{\exp((\Delta E_w - \Delta E_j)/kT_e)}{T_e} \tag{44}$$

where β is a function of transition rates, autoionization rates, and effective collision strength. ΔE$_w$ is the energy separation between the levels of the line w and ΔE$_j$ is the energy separation of the levels of the line j.

12. Database

Most of the atomic data calculated using the Superstructure and DW programs are available in the CHIANTI database (Young et al. 1998; Dere et al. 1997). Effective collision strengths for a number of ions obtained from DW or R-matrix calculations are given in Lang (1994).

13. Conclusions

A large number of DW calculations have been carried out over the years and just a few have been mentioned here. As the computational facilities improve so does the scope of the calculations: a larger number of configurations and incident partial waves can now be used in computing atomic data for an ion of interest. We have assumed a constant element abundance and a steady state coronal equilibrium condition in the calculations of intensities of various emission lines in spite of the doubts expressed by Feldman (1993). This is an interesting paper and questions the validity of a few other assumptions too. Physical properties can be inferred from a comparison of the calculated intensities with the observed ones. It is clear that the DW calculations are reasonably accurate for highly charged ions and at high electron temperatures. The Bowen fluorescence mechanism and optical depth effects can be considered in the calculation of line intensities. Unidentified lines in observed spectra can also be identified using such calculations. Most EUV and X-ray lines are emitted only when the plasma is at high temperatures and therefore the DW calculations should be suitable in such cases. Moreover, such calculations as discussed here are always required in the absence of experimental determination of all the enormous data needed to analyze the solar and astrophysical observations.

Acknowledgments. Thanks are extended to Dr. W. Eissner who, over the years, has been generous in making available to me the updated programs, and to Dr. J. L. R. Saba for helpful comments. This paper is dedicated to the memory of Dr. S. O. Kastner with whom I collaborated for a quarter of a century. His death in August, 1999 brought to an end a very fruitful association.

References

Acton, L.W., Bruner, M.E., Brown, W.A., Fawcett, B.C., Schweizer, W., and Spear, R.J. 1985, ApJ 291, 965.

Arnaud, M. and Rothenflug, R. 1985, ApJS 60, 425.

Behring, W.E., Cohen, L. and Feldman, U. 1972, ApJ 175, 493.

Behring, W.E., Cohen, L., Feldman, U. and Doschek, G.A. 1976, ApJ 203, 521.

Bhatia, A.K. and Doschek, G.A. 1992, ADNDT 52, 1.

— 1993, ADNDT 53, 195.

— 1993a, ADNDT 55, 315.

— 1993b, ADNDT 55, 281.

— 1993c, ADNDT 55, 195.

— 1995, ADNDT 60, 145.

— 1995a, ADNDT 60, 97.

Bhatia, A.K. and Eissner, W. 2000, ADNDT (submitted)

Bhatia, A.K., Feldman, U., and Seely, J.F. 1985, ADNDT 32, 435.

— 1986, ADNDT 35, 319.

— 1986a, ADNDT 35, 449.

— 1987, ADNDT 36, 453.

Bhatia, A.K. and Kastner, S.O. 1985, Solar Phys. 96, 11.

— 1988 ApJ 332, 1063.

— 1992, ApJS 79, 139.

— 1993, ADNDT 54, 133.

— 1999, ApJ 516, 482.
Bhatia, A.K., Kastner, S.O. and Behring, W.E. 1982, ApJ 257, 998.
— 1983, ApJS 53, 129.
Bhatia, A.K. and Mason, H.E. 1980, MNRAS 190, 925.
— 1997, ADNDT 66, 119.
Bhatia, A.K., Mason, H.E., and Blancard, C. 1997, ADNDT 66, 83.
Bhatia, A.K. and Thomas, R.J. 1998, ApJ 497, 483.
Bhatia, A.K., Seely, J.F. and Feldman, U. 1987, ADNDT 36, 453.
— 1989, ADNDT 43, 99.
Bhatia, A.K. and Young, 1998, ADNDT 68, 219.
Brickhouse, N.S., Raymond, J.C. and Smith, B.W. 1995, APJS 97, 551.
Brosius, J.W., Davila, J.M., and Thomas, R.J. 1998, ApJS 119, 225
Brosius, J.W., Thomas, R.J. and Davila, J.M. 1999, ApJ 526, 494
Brown, G.V., Beiersdorfer, P., Liedahl, D.A., and Widman, K. 1998, ApJ 502, 1026.
Burgess, A. and Sheorey, V.B. 1974, J. Phys. B 7, 2403.
Capriotti, E.R. 1965, ApJ 142, 1101.
Colon, E.S. Keenan, F.P. and Aggarwal, K.M. 1992, Phys. Scripta 46, 518.
Cook, J.W., Keenan, F.P., Bhatia, A.K. 1994, ApJ 425, 861.
Dere, K.P., Landi, E., Mason, H.E., Monsignori Fossi, B.C., and Young, P.R. 1997, A&AS 125 149.
Doschek, G.A. 1985, in "Autoionization, Recent Developmenta and Applications" (A. Temkin ed.), Chap. 6, Plenum Press, New York.
Doschek, G.A., Feldman, U. and Bhatia, A.K. 1991, Phys. Rev. A 43, 2565
Eissner, W. 1998, Compt. Phys. Commun. 114, 295.
Eissner, W., Galavis, M.E., Mendoza, C. and Zeippen, C.J. 1999, A&AS 137, 165.
Eissner, W., Jones, M. and Nussbaumer, H. 1972, Compt. Phys. Commun. 8, 270.
Eissner, W. and Seaton, M.J. 1979, J. Phys. B 5, 2187.
Fawcett, B.C., Jordan, C., Lemen, J.R., and Phillips, K.J.H. 1987, MNRAS 225, 1013.
Feldman, U. 1992, Physica Scripta 46, 202.
— 1993, Physica Scripta T47, 128.
Feldman, U. and Doschek, G.A. 1977a, J. Opt. Soc. Am. 67, 726.
— 1977b, ApJ 212, L147.
Feldman, U., Doschek, G.A. and Seely, J.F. 1985, MNRAS 212, 41P
Feldman, U., Purcell, J.D. and Dohne, B. 1987, Special NRL publication, available from NRL, Library of Congress Card Catalog No. 87-63602
Hagelstein, P.L. and Jung, R.K. 1987, ADNDT 37, 121.
Harrison, R.A. et al. 1995 Solar Phys. 162, 233.
Huang, L.K., Lippman, S., Yu, T.L., Stratton, B.C., Moos, H.W., Finkenthal, M., Hodge, W.L., Rowan, W.L., Richards, B., Phillips, P.E. and Bhatia, A.K. 1987, Phys. Rev. A 35, 2919.
Jordan, C. 1969, MNRAS 142, 501.
Judge, P.G. 1998, ApJ 500, 1009.
Kastner, S.O. and Bhatia, A.K. 1979, A&A 71, 211.
— 1984, ApJ 287, 945.
— 1986, Comments on Atomic and Molecular Physics 18, 39.
— 1987, Physical Scripta RS5, 76.
Kastner, S.O., Behring, W.E. and Bhatia, A.K. 1983, ApJS 53, 129.
Kastner, S.O. and Kastner, R.E. 1990, JQSRT 44, 275.
Lang, J. 1994, (Special Editor), ADNDT 57, 1.

Mason, H.E. Doschek, G.A., Feldman, U. and Bhatia, A.K. 1979, A&A 73, 74.
Mason, H.E. and Storey, P.J. 1980, MNRAS 191, 631.
McKenzie, D.L., Landecker, P.B., Broussard, R.M., Rugge, H.R. and Young, R.M. 1980, ApJ 241, 409.
Molinovsky, M. and Heroux, L. 1973, ApJ 181, 1009.
Parkinson, J.H. 1975, Solar Phys. 42, 183.
Pellan, J. and Berrington, K.A. 1995, A&AS 110, 209.
Phillips, K.J.H., Bhatia, A.K., Mason, H.E. and Zarro, D.M. 1996, ApJ 466, 549.
Phillips, K.J.H., Greer, C.J., Bhatia, A.K., Coffey, I.H., Barnsley, R. and Keenen, F.P. 1997, A&A 324, 381.
Phillips, K.J.H., et al. 1982, ApJ 256, 774.
Phillips, K.J.H., Greer, C.J., Bhatia, A.K. and Keenen, F.P. 1996, ApJ 469, L57.
Rugge, H.R. and McKenzie, D.L. 1985, ApJ 297, 338.
Saba, J.L.R., Schemlz, J.T., Bhatia, A.K. and Strong, K.T. 1999, ApJ 510, 1064.
Saraph, H.E. 1978, Compt. Phys. Commun. 15, 247.
Saraph, H.E. and Eissner, W. 2000, Compt. Phys. Commun. (to be published)
Schmelz, J.T., Saba, J.L.R. and Strong, K.T. 1992, ApJ 398, L118.
Thomas, R.J. and Neupert, W.M. 1994, ApJS 91, 461.
Vernazza, J.E. and Reeves, E.M. 1978, ApJS 37, 485.
Wood, K. and Raymond, J. 2000, ApJ (accepted)
Young, P.R., Landi, E., and Thomas, R.J. 1998, A&A 329, 291.
Young, P.R., Mason, H.E., Bhatia, K.A., Doschek, G.A. and Thomas, R.J. 1996, Proceedings of IAU No. 152, Eds. Bowyer and Malina, p.583
Zhang, H. and Sampson, D.H. 1989, ADNDT 43, 1.
Zhang, H., Sampson, D.H., Clark, R.E.H., and Mann, J.B. 1987, ADNDT 37, 17.
Zhitnik, I.A., Kuzin, S.V., Oraevskii, V.N., Pertsov, A.A., Sobel'man, I.I., and Urnov, A.M. 1998, Astron. Lett. 24, 819.